Extreme Mechanics Letters 43 (2021) 101202

Contents lists available at ScienceDirect

Extreme Mechanics Letters

journal homepage: www.elsevier.com/locate/eml

Investigating the mechanical response of microscale pantographic structures fabricated by multiphoton lithography

Zacharias Vangelatos [a], M. Erden Yildizdag [b], Ivan Giorgio [c], Francesco dell'Isola [c,*], Costas Grigoropoulos [a,*]

[a] Department of Mechanical Engineering, University of California, Berkeley, CA, 94720, USA
[b] Faculty of Naval Architecture and Ocean Engineering, Istanbul Technical University, Istanbul, 34469, Turkey
[c] International Research Center for the Mathematics and Mechanics of Complex Systems, University of L'Aquila, Italy

ARTICLE INFO

Article history:
Received 14 October 2020
Received in revised form 13 January 2021
Accepted 24 January 2021
Available online 4 February 2021

Keywords:
Multiphoton lithography
Hyperelasticity
In situ SEM microindentation
Pantographic structures
FEA modeling
Mechanical Metamaterials

ABSTRACT

The design of micromechanical devices that can facilitate large but recoverable deformations requires a mechanical behavior that embosoms hyperelasticity. While multiphoton lithography is the epitome of microscale fabrication, the employed materials demonstrate a linear elastic response accompanied by limited ductility. In this study, we investigate how this hindrance can be circumvented through the design of microscale pantographic structures. Pantographs possess riveting hyperelastic response inherited by their structural design, providing exorbitant reversible deformations. To prove the utility of pantographs in microscale design, finite element analysis simulations are performed to unravel the behavior of the structure as a function of its geometrical parameters. In addition, to evaluate the microscale modeling, specimens are fabricated with multiphoton lithography in a push to pull up configuration to accomplish in situ SEM microindentation tensile testing due to compression. Our findings are adduced to expound how the pantographic structures can embrace hyperelastic response even at the microscale, elucidating their feasibility for structural members in micromechanical devices that require reversible large deformations.

© 2021 Published by Elsevier Ltd.

1. Introduction

The implacable progress in 3D printing technologies has enabled the fabrication of complex 2D or 3D structures, possessing unprecedented properties. Specifically, these remarkable advances in microscale printing have enabled the design of MEMS devices, microrobotic devices [1,2], scaffolds for tissue engineering and the investigation of cellular malfunction [3] and even biomimetics and bioimplants [4]. However, despite the fact that for such domains fabrication techniques such as FIB milling [1], microstereolithography [5] or direct ink writing are highly efficient, they cannot be employed for the fabrication of highly complex 3D structures that possess features with nanoscale resolution. To surmount this inherent challenge, the fabrication of 3D complex microscale structures can be accomplished by additive manufacturing techniques such as multiphoton lithography (MPL) [6]. MPL has resolved the fabrication of complex 3D structures with even 200 nm features resolution [7], spanning in mm^2 surface areas [8]. Hence, it can furnish the design of micro/nanoscale structures and devices. Characteristic examples that have illuminated the utility of this technique are hierarchical structures that are the simulacrum of perplexing living organisms, such as marine diatoms [9]. Another instantiation is the exceptional mechanical response of microlattice and microplate structures, demonstrating either controlled buckling and directional stiffness or isotropic behavior [7]. Furthermore, it has been employed to generate 3D scaffolds and unveil the 3D cellular response of living cells or tissue [10].

Despite the deep perspicacity into the complexity of the designs that can be fabricated with MPL, there are still innate challenges associated with the employed materials. More specifically, the photoresists utilized in MPL are polymer ceramic hybrids, conferred with linear elastic response and a limited degree of ductility beyond the yielding point. While their fracture is brittle due to crazing [11], the design of architected materials can impede the brittle fracture through tailored 3D buckling that can lead to the densification and subsequently the abrupt increase of the apparent ductility of the material [12,13]. Regarding the increase of strength of the fabricated specimens, post processing techniques such as pyrolysis have been employed, ablating the polymeric part to create a nanoscale ceramic structure. Such specimens can have 20% of the original volume and they can reach the theoretical strength of the glassy carbon [7], even though they are comprised of a nanolattice geometry. In addition,

* Corresponding authors.
E-mail addresses: francesco.dellisola@uniroma1.it (F. dell'Isola), cgrigoro@me.berkeley.edu (C. Grigoropoulos).

https://doi.org/10.1016/j.eml.2021.101202
2352-4316/© 2021 Published by Elsevier Ltd.

to enhance the ductility of the brittle constituent, atomic layer deposition assisted by plasma etching has been employed to create hollow nanotubes with thickness that is a few tens of nm [14]. These hollow ceramic structures demonstrate exceptional ductility and resilience to plastic collapse, despite the fact that the employed material is a brittle ceramic. Nevertheless, microscale engineering applications require components that can sustain large but reversible deformations [15]. Moreover, designs that exhibit multiple equilibrium positions for controlled wave propagation or bistability [16] are encompassed by the constraint that the utilized material is hyperelastic and does not yield or fracture during the multiple loading cycles. Therefore, the fact that the materials used in MPL do not demonstrate hyperelasticity obstructs their utility for the aforementioned applications. Even though shape memory alloys can be employed at these length-scales and can facilitate large reversible deformations [1,17], it is extremely arduous to process them in micro/nanoscale in the 3D space, limiting the reported results to 2D designs. Hence, the engineering prescience and profundity of the designer must surpass this design constraint.

To supersede the behavior of the bulk material, various different types of metamaterial structures have been proposed [18–21]. Regarding the hyperelastic response of architected materials, one of the most thoroughly studied categories of mechanical metamaterial structures are the pantographic structures [22,23]. These geometries are comprised of arrays of orthogonal beam members that are concatenated together by pivots. The pivots enable the relative rotation of the beams. These structures can undergo extremely large, but recoverable, deformations.

Besides, in macroscale, it has been shown that such structures can be modeled with a second gradient continuum, rendering the strain energy a function of the second gradient of the displacement [24,25]. From a theoretical standpoint, this sublime result reveals that the ideas initiated by different mechanical models regarding higher gradient elasticity since the late 19th century are conceivable and feasible [26] with advanced additive manufacturing fabrication techniques. Ergo, different higher gradient models have been developed to investigate the mechanical behavior of pantographs [27]. Furthermore, simple first gradient models (i.e. models that the strain energy is only dependent on the first gradient of displacement) cannot depict the mechanical response of the material, since second gradient elasticity becomes more predominant in materials with a specific tactical ordonnance of "fiber" constituents. Hence, the nonlinear mechanical response of the pantograph has been conveyed even when the employed 3D printing materials are highly brittle. Thus, the pantographic structures are compelling due to the fact that they constitute a synthesis for second gradient 2D continua. To attain the required macroscopic deformation energy, the specific rescaling of micro-stiffnesses is required. Therefore, there are constraints on the feasible variations for obtain any desired macro-behavior. While large elongations in the elastic regime have been explored [28], optimization is crucial to control the range of elastic deformations under specific imposed constraints. To accommodate this, optimization procedures have been employed in the context of pantographic micro-structures, demonstrating that the geometry of the considered structure can be optimized using as control parameters some of the characteristic lengths of the constituent elements [29]. To design microstructures realized by additive manufacturing, the construction specifications of the inherent structural members have to be determined. In particular, it is critical to define the elastic pivots having small torsional stiffness. To accomplish this, an expedient procedure of structural optimization would be the use of beams with variable thickness with an alternation of very stiff parts and very compliant ones [30]. The softest parts of the beams can be regarded as elastic hinges, and design schemes like those can be efficiently implemented with meagre computational cost. In addition, it has been demonstrated that they also incur more complex responses, such as the Poynting effect, out-of-plane or 3D buckling modes and coupling deformation modes [31]. To comprehend this behavior, a panoply of other analytical [32] and numerical approaches has been proposed, such as the Hencky-type discrete model or the nonlinear Euler–Bernouilli beam modeling [33]. These models have also been employed to ameliorate the inordinate computational cost of the FEA simulations that is required to solve the various boundary value problems substantiated in these structures. Consequently, these computational tools, embracing higher order terms, have successfully diminished the computational cost that is needed to solve complex structural problems even beyond pantographic structures. This extensive investigation of the mechanical behavior of pantographic structures has rendered them a celebrated paradigm of designed, modeled and experimentally validated hyperelastic architected geometries. Hence, their intriguing behavior should also beget a viable candidate for large deformations in microscale.

Despite this unprecedented progress in the design of pantographic structures in macroscale, assimilating them in microscale in still tenuous. These types of structures could be considered as a potential candidate for the design of MEMS microdevices, acoustic metamaterials [34] or even microscale implants [35] that require nonlinear elastic deformations without plasticity.

In this paper we aim to expand the study of microscale pantographic structures and investigate their utility as hyperelastic structures in microscale. More specifically, through MPL, we fabricate a push to pull out mechanism to achieve tensile tests by applying compression to the structure [36]. MPL enables the fabrication of pantographic unit cells, with fixed beams and pivots. Through in situ SEM-microindentation experiments we are able to observe deformations in the nanoscale regime. In addition, we can juxtapose the mechanical performance with the macroscopic force–displacement response and the dominating deformation modes in the structure. Furthermore, we perform finite element analysis (FEA) simulations to evaluate the sensitivity of the mechanical response to the geometrical parameters of the unit cell. We prove that the experimental response of up to 25% deformations of pantographic unit cells can be modeled through hyperelasticity, even though the base material is not hyperelastic. These findings aim to accentuate the characterization and modeling of pantographs in microscale for applications that necessitate nonlinear elastic deformations and pave the way to incorporate specimens fabricated by MPL in this endeavor.

2. FEA modeling of microscale pantographs

The design of the pantographic unit cells is delineated in Fig. 1(a). The unit cells are comprised of beam members of width w_b and height h_b oriented at 45^o with respect to each other. Each beam is connected with the proximal one through three pivots at the edges and its center. The pivots have radius r_p and height h_p. While in macroscale pantographs the pivots can enable the rotation of the beams through angular sliding [27], this mechanism cannot be realized in microscale with MPL. The reason for this constraint is that the material is polymerized through subsequent laser beam scans and the respective components are not assembled together. Hence, in our design, the specimen is fabricated with fixed beam supports. Nevertheless, as we will show later, the pivots still dominate the mechanical response. Since the in-situ microindentation experiments can only be conducted under compression, to realize tensile tests an acute mechanism needs to be utilized. To accomplish this, we employed a push to pull

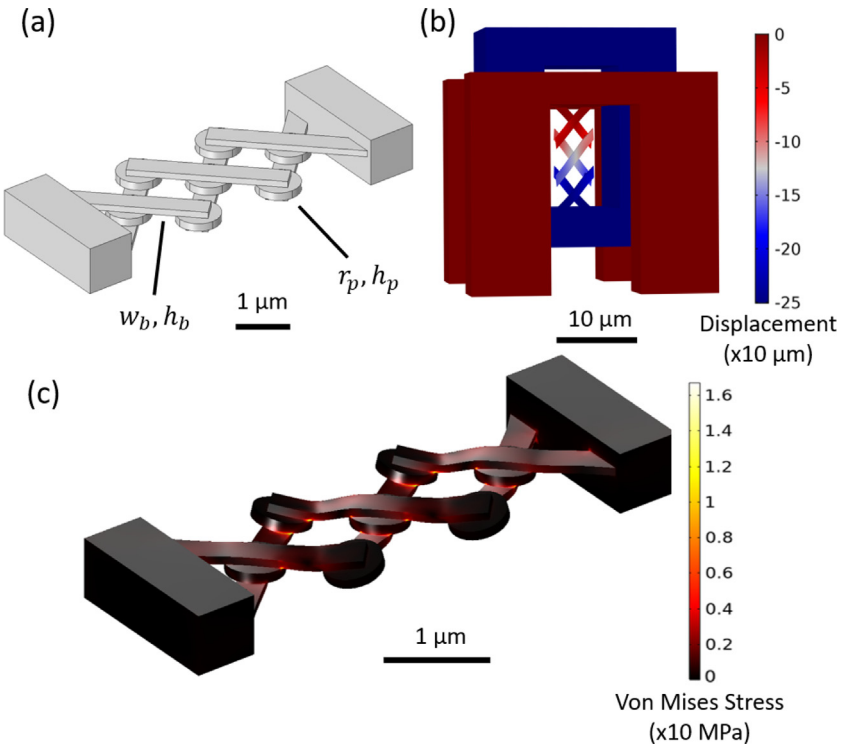

Fig. 1. Modeling of microscale pantographic structures. (a) The pantographic unit cell, comprised of beam members with width w_b and height h_b, arranged on two planes and with relative angle 45°. The beam members on the two planes are connected with a pivot of radius r_p and height h_p at the center and the edges of the beams. (b) FEA simulation of the pantographic unit cell on the tensile mechanism. The two parts of the mechanism have a uniform displacement, ensuring that they do not affect the mechanical response of the unit cell. (c) FEA simulations of the pantographic unit cell under tension. It is observed that the maximum stress of the specimen is localized in the pivots, dominating the mechanical response of the material through torsion.

out mechanism that has been previously employed for tensile specimens in microscale [36]. Specifically, the unit cell is attached at one end on a base that is fixed to the substrate and at the other end on a rectangular base that can be translated under compression, thus enabling the manifestation of tensile deformation on the tested structure. Fig. 1(b) demonstrates the FEA simulation of the mechanism under compression of the upper base. It is shown that the deformation field has a constant and uniform distribution on the mechanism. Therefore, the mechanical response of the unit cell is impervious of localized deformation effects that would be caused by the tensile mechanism. Therefore, conducting such measurements will not distort the actual behavior of the pantographic structure.

In order to numerically investigate the mechanical behavior of the microscale pantograph in this study, FEA simulations were performed using the commercial FEA software COMSOL Multiphysics®. A characteristic 3-D FEA model of the microscale pantograph with pivot radius $r_p = 1.35\,\mu m$, pivot height $h_p = 0.6\,\mu m$, beam width $w_b = 1.25\,\mu m$ and beam height $h_b = 0.5\,\mu m$ was generated and is precented in Fig. 1(c). A hyperelastic model available in COMSOL Multiphysics®, namely the Yeoh model, was adopted in the simulations. In this model, the strain energy density is defined as follows

$$W = c_1(I_1 - 3) + c_2(I_1 - 3)^2 + c_3(I_1 - 3)^3 \tag{1}$$

where c_1, c_2 and c_3 are the material parameters of the constitutive equation and I_1 is the first invariant of the Cauchy–Green deformation tensor $\mathbf{C}$. The main reason that the Yeoh model was selected is that the mechanical behavior of pantographic structures seems to be described fairly well compared to other hyperelastic models, as it has been highlighted in previously reported work [37]. Accordingly, the 2nd Piola–Kirchhoff stress tensor can be calculated by the following equation

$$\mathbf{S} = 2\frac{\partial W}{\partial \mathbf{C}} \tag{2}$$

Hence, the stress field and the displacement field in the structure can be calculated by solving the corresponding boundary value problem of the linear momentum balance. As it will be discussed later, even though the Yeoh's model has been employed for macroscale specimens, it can also capture the convex behavior of the microscale results, while other tested models such as the Neo-Hookean or Mooney–Rivlin hyperelastic constitutive models could not capture the experimental results. The numerical computations were conducted with a mesh of 90,235 tetrahedral elements and 351,255 degrees of freedom. To simulate the tensile test of the specimen, a 2.5 μm displacement was applied in a stepwise manner, and the material parameters were selected as follows: $c_1 = 3.29 \times 10^9$, $c_2 = 2.02 \times 10^{10}$, and $c_3 = 6.10 \times 10^{10}$. As it will be explained in the next section, the numerical values of these parameters were selected based on a parametric analysis to match the experimental results. An iterative process was addressed to obtain the material parameters. Hence, the presented values were found to closely match the experimental results. As it will be described next, these constitutive parameters were also employed to conduct a sensitivity analysis in the specimen by varying the dimensions of the characteristic geometric parameters of the unit cell. The force–displacement behavior was obtained through the integration of the reaction forces at the fixed end of the specimen for each corresponding displacement. In Fig. 1(c), the calculated von Mises stresses are presented when the displacement is equal to 2.5 μm.

3. Fabrication and testing

To evaluate the designed tensile response of the modeled pantograph, benchmark test structures were fabricated by MPL,

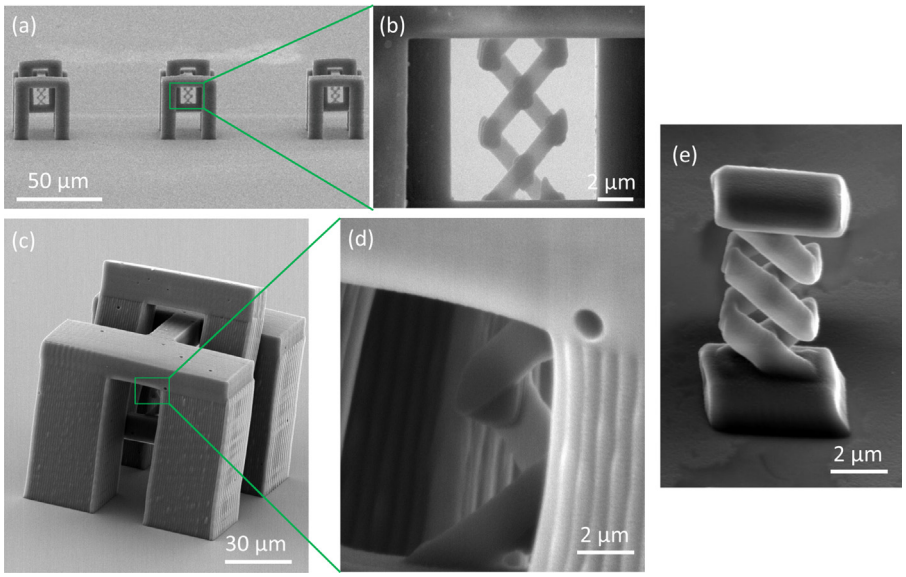

Fig. 2. Fabricated micropantographic specimens through MPL. (a) Front view of fabricated unit cells in the tensile mechanism. (b) High magnification image of the unit cell. (c) Side view of the specimen, showing the thickness of the pivot and the two parts of the tensile mechanism. (d) High magnification image of the pivot to verify that the dimensions are in agreement with the fabrication parameters and the simulations. (e) The pantographic unit cell without the tensile mechanism, showing the connection of the beam members on the two different planes through pivots at the edges and the center.

presented in Fig. 2. The experimental apparatus utilized for this process has been reported in previous work with respect to the fabrication of microscale metamaterial structures [13]. More specifically, the fabrication conditions for the preparation of the samples were 2 mW output laser power of a Ti:Sapphire femtosecond laser (FemtoFiber pro NIR) and 10 μ m/s scanning speed for the stages that translate the sample such that the laser beam can "write" the geometry into the photoresist. Since each laser pulse creates a voxel of polymerized material, the laser beam was passing through the same direction at least four times to increase the rigidity of the structures. The material that was used is the commercial photoresist SZ2080TM, originated from FORTH. The fabrication conditions were selected such that the viscous effects of the material are diminished based on material characterization that has been reported elsewhere [38]. Further details about the preparation of the material can be found elsewhere [6]. Fig. 2(a) shows multiple specimens fabricated in the push to pull out mechanism (Fig. 2(b)). The dimensions of the unit cells match the ones of the simulations that were provided in the previous section to calculate the material parameters. Fig. 2(c) shows the side of one of the specimens demonstrating the pivot dimensions (Fig. 2(d)). Fig. 2(e) shows the pantographic unit cell detached from the tension mechanism, illuminating that all of the beam members and pivots have the same dimensions, respectively.

To conduct the mechanical experiments, nanoindentation experiments were performed. The nanoindenter (Hysitron P188 SEM PicoIndenter, Bruker), which is mounted inside an SEM, was applying a compressive force to the top base of the structure, pulling it downwards and applying a tensile deformation to the unit cell. The specimens are positioned such as the front view is visible from as in Fig. 2b to enable the in situ observation of the deformation of the unit cell. To avert any strain rate effects during the deformation of the material, the specimens were loaded with a constant rate of 10 nm/s until 25% uniaxial strain. The range of the deformation was selected to be congruous with the dimensions of the tensile mechanism. Higher tolerance in the translation of the upper base would precipitate tilting and out of plane deformation, tottering the unit cell and providing egregious experimental results. To ensure that the experimental results are repeatable, eight specimens were tested five times each, and the average curve of all the results was obtained. The strain rate was selected to obstruct the development of any instantaneous viscoelastic effects in the material and reassure the feasibility of the theoretical model. The loading and unloading stages of the specimen revealed extremely small close loops, which were on the verge of statistical error that the indenter can capture. In addition, close observation of the recorded videos showed that the specimens were returning to the initial equilibrium position before loading was applied.

4. Results and discussion

To evaluate the mechanical response of the tested specimens, it is critical to comprehend the mechanical response that was observed in the FEA simulations. Fig. 1(c) shows that the highest stress distribution is emerged at the pivots, while the von Mises stress at the other members of the specimen is minuscule. This result alludes that the geometric properties of the pivots must have an imperative role to comprehend the mechanical behavior of pantographic structures and they must be the dominating constituents in the mechanical response. Consequently, to obtain a better understanding regarding the mechanical behavior of the structure, a sensitivity analysis was performed with respect to the four main geometric properties, namely the pivot radius (r_p), the pivot height (h_p), the beam height (h_b), and the beam width (w_b). This analysis may also be useful to provide an exegesis regarding discrepancies that may occur due to the printing and testing processes regarding variations in the dimensions of the printed specimens. In each case, the targeted parameter was varied while the other parameters were preserved fixed, and using the same material parameters given in Section 2 in all of the simulations. The obtained results for the sensitivity analysis are presented in Fig. 3. In Figs. 3(a) and 3(b), the obtained force–displacement curves are presented with variation in the pivot radius and the pivot height, respectively. The stiffness of the pantographic structure decreases significantly with decreasing the pivot radii, and ostensibly, the concavity of force–displacement curves changes with lower values of the pivot radius.

Especially for $r_p = 0.6$ and 0.4 μm, the force–displacement curves are concave up as opposed to the concave down curves

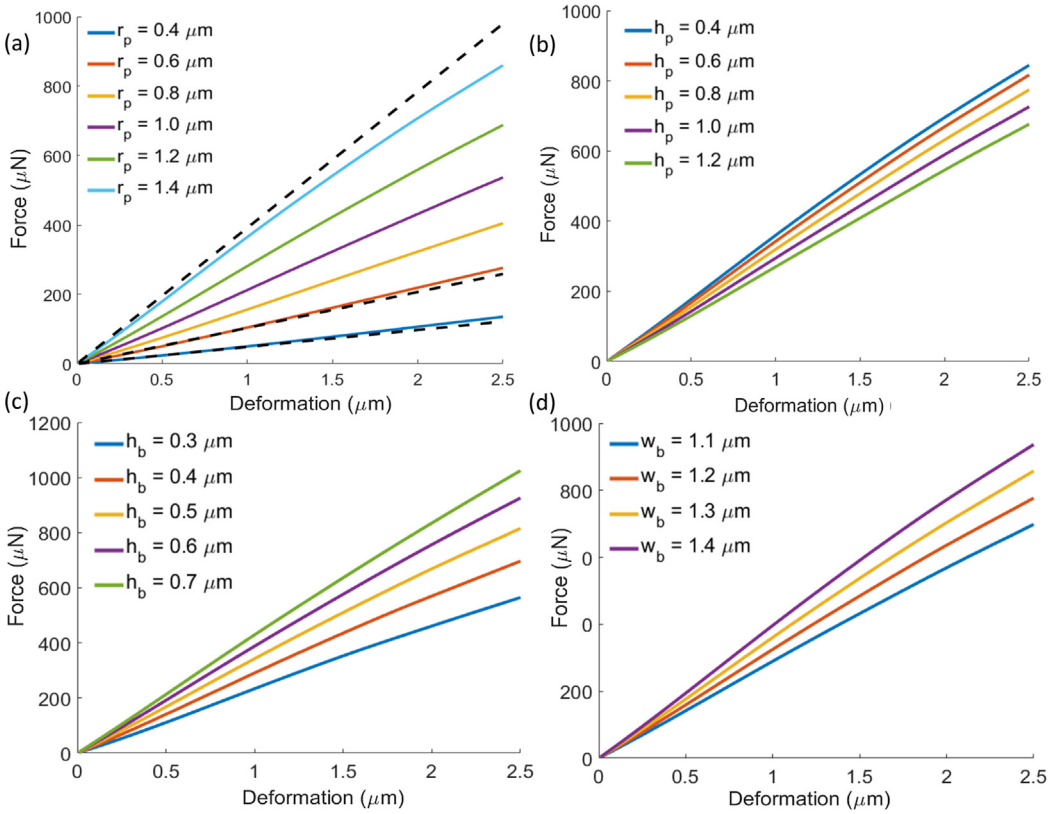

Fig. 3. Sensitivity analysis of the mechanical performance based on the geometric parameters. (a) Variation of the mechanical response due to different pivot radii. It is observed that the response is highly sensitive to the radius, with substantial variation in both the magnitude and convexity of the force–displacement curve, since the torsion of the pivots dictates the mechanical response. The dashed lines are the linear part (i.e. the second derivative) of a second degree polynomial that was used to curve fit the simulation results. For $r_p = 0.4$ the second derivative is 2.38, while for $r_p = 1.4$ the second derivative is -17.30. (b) Variation of the mechanical response due to different pivot thicknesses. The response is not highly sensitive to the thickness, since significant variation will be discernible for longer pivots. (c) Variation of the mechanical response due to different beam heights. There not commensurate sensitivity with the pivot radius. since the beams rotate due to the pivot deformation. (d) Variation of the mechanical response due to the beam length. Again, since bending of the beam members is not the dominant mechanism, the response is not highly sensitive to the variation of the length.

obtained for higher values of pivot radius. To allude this, each curve was curve fitted by a second polynomial and its linear part is plotted by dashed lines in Fig. 3(a). This conveys that the curves diverge from linearity and the value of the second derivative shifts the convexity of the curve from one verge of the line to the other. Even though the R^2 is close to 1 for all of the curves, a second degree polynomial curve fitting should only be employed to limn the variance of the convexity and not for any other physical interpretation of the simulation results. As it is expected, a decrease in the height of the pivot will lead to a stiffer behavior for the pantographic structure, as it is observed in Fig. 3(b). Even though the variance of the pivot height is ranging between 1.2 μm and 0.4 μm, the differences in the computed reaction forces are not as significant as the variance in the behavior that is observed for the variation in the pivot radius. Moreover, in Figs. 3(c) and 3(d), the results are given for variation in beam height and beam width, respectively. It is evident that the variation of the geometric parameters associated with bending do not lead to substantial changes in the resulted force–displacement curves, corroborating the dominance of the pivots in the resulted mechanical response. Hence, as in macroscale pantographs, bending is not the driving mechanism, but instead the torsion of the pivots.

Fig. 4 shows the tested specimens and the resulted force–displacement curve. As it is shown in Fig. 4(a), a compressive load is applied by the indenter to the tensile mechanism and the SEM is focused on the pantographic unit cell. A representative video recording of the testing is provided in the Supplementary Data (Video 1). The specimen is loaded under 25% uniaxial deformation and then it goes back to the reference configuration. Fig. 4(b) shows the comparison between the experimental result and the numerical simulation employing Yeoh's hyperelastic model.

Our results show a close match between the experiments and simulations, validating the hyperelastic behavior of microscale pantographic structures for this range of deformation. A careful observation of the experiments also illuminated that the dominant mechanism is torsion in lieu of the bending of the beams, a result that is consonant with the FEA simulations. Hence, based on both the numerical and the experimental results, bending is not the dominant mechanism for the examined microscale pantographic structure. Therefore, the control of the mechanical behavior for these types of structures should solely focus on the geometry of the pivot. This result shows that even though the pivots are fixed in MPL fabrication, the capability of the pantographic structure to possess hyperelastic behavior is also feasible at the microscale. To put this mechanical performance into perspective, the behavior of the bulk material was also evaluated. The experimental result of the von Mises stress as a function of the strain for the bulk material, along with the deformation of the structure that was simulated up to 35%, are presented in Fig. 4(c). It is evident that the bulk material possesses brittle linear behavior that can sustain stress equal 55.89 ±2.95 MPa at strain 0.7% when fracture commences. This response is consistent with the fabrication conditions we employed in our previous work and the fractographies that revealed brittle fracture [11]. However, the simulation of the pantographic structure shows that the von

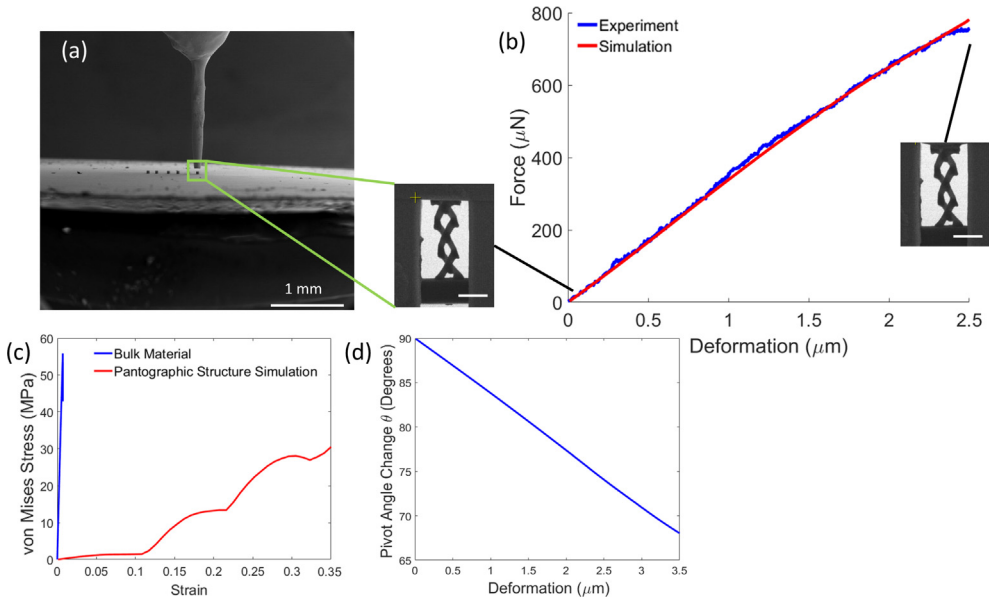

Fig. 4. In-situ microindentation testing on the fabricated specimens. (a) Far front view of the specimens next to the indenter right before the testing inside the SEM. (b) Comparison of the average experimental curve with the FEA simulations until 25% deformation. There is close match between experiments and simulations, elucidating that the Yeoh hyperelastic model can delineate the mechanical response of the microscale pantograph. (c) Comparison of the von Mises of the bulk material in juxtaposition with the FEA simulation of the pantographic structure for 35% deformation. The bulk material demonstrates brittle behavior and linear elastic response, whereas the pantographic structure can sustain stresses below the strength of the material at a significantly larger regime of deformations. (d) The angle variation between two perpendicular material lines at the pivot. The manifestation of large deformation is caused by the large rate of angle change of the pivot which is 32 degrees at 35% deformation.

Mises stress reaches 30.5 MPa, enabling the structure to possess irreversible deformations without failure. Thus, despite the fact that the material used in MPL is not hyperelastic, the response of the pantographs can be modeled with Yeoh's hyperelastic model. Furthermore, the deformation of the pivot was evaluated to assess the effect of the rotation on the deformation of the structure. The simulation result is demonstrated in Fig. 4(d). The angle θ is the angle between two material lines on the pivot that are perpendicular (90°) in the undeformed configuration. It is shown that the angle variation is linear throughout the deformation of the structure, rising to 32 degrees at the maximum deformation. Hence, larger dimensions on the pivot can result in an abrupt change of the deformation, a result which is consistent with the effect of r_p conveyed in Fig. 3(a) and the initial assumption of the physical mechanism. Nevertheless, pantographic structures can be deformed at even higher deformations as it has been presented in previous work [24,25], reaching 85% reversible deformation. To experimentally realize these extraordinaire results, larger specimens comprised of hundreds of beam members must be fabricated. Hence, more advanced techniques in MPL microfabrication should be employed [8], providing a new avenue to study the hyperelastic behavior of architected metamaterials. However, the analysis of the mechanical performance at even smaller length scales would be of cardinal significance. More specifically, techniques such as pyrolysis, as it was addressed before [7], and stimulated emission depletion MPL [39] enable the fabrication of members at a few tens of nm. It must be pointed out that the pantographic behavior of the examined structure is based on the particular arrangement of the constituent elements that allow, in the ideal case, a relative motion between them without any expense of energy. This instance is also known as a floppy mode. This peculiarity can be described at rigorously with a second gradient continuum model if many unit cells of such a pantographic mechanism are assembled to create an array. Nonetheless, a first gradient model can be employed at the constituent elements level. The asymptotic homogenization procedure illuminates how the constitutive parameters at the macroscopic level are to be determined in terms of the constitutive parameters at the micro-level [27]. The rescaling laws of micro-constitutive parameters, depending on the size of the homogenization cell, are determined to provide the onset of second gradient effects at the macro level. Specifically, for pantographic sheets, and if ϵ denotes the distance between the closest pivots, the rescaling that characterizes 2D continuum models requires that the beam bending stiffness, the beam extensional stiffness, and the torsional stiffness of the pivots must rescale respectively with ϵ^0, ϵ^0, and ϵ^2. Hence, the torsional stiffness of the pivots must be very weak compared to the bending stiffness, and the bending stiffness must vary with epsilon along with the extensional stiffness. Therefore, when the aforementioned rescaling laws are followed and until classical mechanics is applicable such that quantum effects do not play a relevant role, then the presented modeling can be used regardless of the size. When the overall scale of the structure is dramatically decreased to scales close to nm, second gradient continuum models are still valid in principle. However, the scale reduction may have another important consequence even when the theory of classical mechanics remains applicable: the inner substructure of the bulk material constituting the pantographic micro-structure, depending on the particular technological process used for constructing it, could have a characteristic length comparable with one of the constituents. Then, the model required for the micro-constituents could be dependent on quantum mechanics or, if classical mechanics applies, to second or higher gradient continuum mechanics. Experimental results [40] at the nanoscale have revealed that higher gradient continuum models can be utilized. Albeit there are no general homogenization results producing second gradient continua from complex micro-structures, some nascent results have been demonstrated [41]. These findings provide us the threshold to reach the following conjectures: (1) Higher-order continua can be obtained at macro-level only when periodical cells are interacting in such a way that any periodic boundary condition for each cell countervails potential higher gradient effects; (2) macro-boundary conditions at the current boundary of the structure must regard the interaction between

the external environment and some cells that are not on the boundary but at a distance of several cells inside, depending on the higher gradient appearing in the deformation energy; (3) to employ higher gradient continua, at the macro level, it is necessary to have high contrast in micro-stiffnesses. Rigorous Gamma-convergence results have been obtained [22], proving that the three listed conjectures are reasonable in the particular case of linear pantographic beams. Moreover, assembling many cells produces a structure described at the overall observation scale as a complete second gradient 1D continuum model [42]. From this perspective, the implemented boundary conditions can be interpreted as the imposition of a displacement on the ends of the structure, to which a constraint on the strain must be added at the same locations. At the scale of the constituent elements, the particular geometry produces a triple-hinged arch at the ends of the structure that is rather stiff. Therefore, the points in correspondence of the triangle wedge have a minimal displacement, and consequently, the overall elongation in these extreme zones is negligible.

In addition, other designs that require large but recoverable deformations, such as bistability [43] should be investigated with respect to the utility of pantographic structures in complex 3D deformations [44]. In the literature such designs are defined as deployable scissor grids [45]. These structures are comprised of the same geometrical constituents as the pantographs of this study and they can possess complex and multiple equilibrium positions even with 3D deformation modes. Characteristic designs have been incorporated in cellular graphene for energy storage and polymer composites for highly wear resistant devices [46]. Despite the fact that a certain degree of stability can be accomplished with fixed pivots, future work should also focus on the improvement of the MPL process such that rotation-free pivots can be accomplished. In addition, since the MPL encompasses a directionality in the fabrication of polymerized structures through subsequent laser scans, this leads to an inherent "fiber-like" pattern in the microstructure of the material. Hence, for specimens comprised of multiple unit cells, higher gradient elasticity could also be realized, as in the macroscale [27]. Therefore, higher gradient elasticity could be employed as a design tool to model MEMS devices and soft microrobotic mechanisms. Specifically, force-sensitive 3D microgrippers have been fabricated by MPL, enabling the precise grasping of minuscule objects through the deformation of helical microsprings [47]. In micro surgical operations that require substantially higher elongation of the instruments, the hyperelastic behavior of the pantographs would prove to be an instrumental repertoire to design such devices. Finally, light-controlled soft microrobots fabricated by MPL can be employed for cell regulation of transfer of microscale specimens [48] at different locations of a large device or even an organ. Encompassing hyperelasticity in such devices will render them more versatile without the constraint of small strains or high material volume to accommodate the required stresses to perform complex tasks.

5. Conclusions

In summary, the hyperelastic behavior of microscale pantographic structures was investigated. FEA simulations along with performed in situ SEM-microindentation tensile tests provided insight into the mechanical behavior of pantographic unit cells. Even though the MPL enables the fabrication of fixed pivots, their torsional response is the dominant mechanism and can still embrace the mechanical response of pantographs observed in macroscale. In addition, it was elucidated that the deformed structures can obtain large reversible deformations, leading to 25% reversible deformation. This hyperelastic behavior can be modeled through Yeoh's hyperelastic model, even though the photoresist material is not hyperelastic. Our findings promulgate the utility of pantographs for microscale applications requiring hyperelastic behavior and just through the utility of the MPL process without any additional fabrication process or materials.

Declaration of competing interest

The authors declare that they have no known competing financial interests or personal relationships that could have appeared to influence the work reported in this paper.

Acknowledgments

This research was partially supported by the National Science Foundation, USA (NSF) under the Scalable Nanomanufacturing (SNM) Program, Grand No. 1449305. The authors thank Dr Vasilia Melissinaki and Dr Maria Farsari, FORTH Greece, for assisting in the fabrication of some of the employed specimens of the present study. The authors also thank Professor P. Hosemann, Department of Nuclear Engineering, University of California, Berkeley, for the availability of his indentation apparatus and Professor David J. Steigmann, Department of Mechanical Engineering, University of California, Berkeley for providing thoughtful feedback regarding the interpretation of the experimental results. The nanoindentation and SEM experiments were conducted at the California Institute of Quantitative Bioscience (QB3 Lab).

Appendix A. Supplementary data

Supplementary material related to this article can be found online at https://doi.org/10.1016/j.eml.2021.101202.

References

[1] M.-S. Kim, H.-T. Lee, S.-H. Ahn, Laser controlled 65 micrometer long microrobot made of Ni-Ti shape memory alloy, Adv. Mater. Technol. 4 (12) (2019) 1900583.
[2] S. Kim, S. Lee, J. Lee, B.J. Nelson, L. Zhang, H. Choi, Fabrication and manipulation of ciliary microrobots with non-reciprocal magnetic actuation, Sci. Rep. 6 (2016) 30713.
[3] Z. Ma, N. Huebsch, S. Koo, M.A. Mandegar, B. Siemons, S. Boggess, B.R. Conklin, C.P. Grigoropoulos, K.E. Healy, Contractile deficits in engineered cardiac microtissues as a result of MYBPC3 deficiency and mechanical overload, Nat. Biomed. Eng. 2 (12) (2018) 955–967.
[4] J. Koffler, W. Zhu, X. Qu, O. Platoshyn, J.N. Dulin, J. Brock, L. Graham, P. Lu, J. Sakamoto, M. Marsala, et al., Biomimetic 3D-printed scaffolds for spinal cord injury repair, Nat. Med. 25 (2) (2019) 263–269.
[5] E. Behroodi, H. Latifi, F. Najafi, A compact LED-based projection microstereolithography for producing 3D microstructures, Sci. Rep. 9 (1) (2019) 1–14.
[6] A. Ovsianikov, J. Viertl, B. Chichkov, M. Oubaha, B. MacCraith, I. Sakellari, A. Giakoumaki, D. Gray, M. Vamvakaki, M. Farsari, et al., Ultra-low shrinkage hybrid photosensitive material for two-photon polymerization microfabrication, Acs Nano 2 (11) (2008) 2257–2262.
[7] J. Bauer, A. Schroer, R. Schwaiger, O. Kraft, Approaching theoretical strength in glassy carbon nanolattices, Nat. Mater. 15 (4) (2016) 438–443.
[8] L. Jonušauskas, D. Gailevičius, S. Rekštytė, T. Baldacchini, S. Juodkazis, M. Malinauskas, Mesoscale laser 3D printing, Opt. Express 27 (11) (2019) 15205–15221.
[9] S. Luo, J.R. Greer, Bio-mimicked silica architectures capture geometry, microstructure, and mechanical properties of marine diatoms, Adv. Energy Mater. 20 (9) (2018) 1800301.
[10] F.A. Pennacchio, F. Caliendo, G. Iaccarino, A. Langella, V. Siciliano, F. Santoro, Three-dimensionally patterned scaffolds modulate the biointerface at the nanoscale, Nano Lett. 19 (8) (2019) 5118–5123.
[11] Z. Vangelatos, K. Komvopoulos, C. Grigoropoulos, Regulating the mechanical behavior of metamaterial microlattices by tactical structure modification, J. Mech. Phys. Solids 144 (2020) 104112.
[12] Z. Vangelatos, C. Li, C. Grigoropoulos, K. Komvopoulos, Comparison of the mechanical performance of architected three-dimensional intertwined lattices at the macro/microscale, Extreme Mech. Lett. (2020) 100930.

[13] Z. Vangelatos, G.X. Gu, C.P. Grigoropoulos, Architected metamaterials with tailored 3D buckling mechanisms at the microscale, Extreme Mech. Lett. 33 (2019) 100580.
[14] L.R. Meza, S. Das, J.R. Greer, Strong, lightweight, and recoverable three-dimensional ceramic nanolattices, Science 345 (6202) (2014) 1322–1326.
[15] B. El Mansouri, L.M. Middelburg, R.H. Poelma, G.Q. Zhang, H.W. van Zeijl, J. Wei, H. Jiang, J.G. Vogel, W.D. van Driel, High-resolution MEMS inertial sensor combining large-displacement buckling behaviour with integrated capacitive readout, Microsyst. Nanoeng. 5 (1) (2019) 1–14.
[16] J.R. Raney, N. Nadkarni, C. Daraio, D.M. Kochmann, J.A. Lewis, K. Bertoldi, Stable propagation of mechanical signals in soft media using stored elastic energy, Proc. Natl. Acad. Sci. 113 (35) (2016) 9722–9727.
[17] M.A. Zainal, S. Sahlan, M.S.M. Ali, Micromachined shape-memory-alloy microactuators and their application in biomedical devices, Micromachines 6 (7) (2015) 879–901.
[18] E. Barchiesi, M. Spagnuolo, L. Placidi, Mechanical metamaterials: a state of the art, Math. Mech. Solids 24 (1) (2019) 212–234.
[19] A. Amendola, G. Carpentieri, L. Feo, F. Fraternali, Bending dominated response of layered mechanical metamaterials alternating pentamode lattices and confinement plates, Compos. Struct. 157 (2016) 71–77.
[20] A. Amendola, C. Smith, R. Goodall, F. Auricchio, L. Feo, G. Benzoni, F. Fraternali, Experimental response of additively manufactured metallic pentamode materials confined between stiffening plates, Compos. Struct. 142 (2016) 254–262.
[21] F. Fraternali, A. Amendola, Mechanical modeling of innovative metamaterials alternating pentamode lattices and confinement plates, J. Mech. Phys. Solids 99 (2017) 259–271.
[22] J.-J. Alibert, P. Seppecher, F. dell'Isola, Truss modular beams with deformation energy depending on higher displacement gradients, Math. Mech. Solids 8 (1) (2003) 51–73.
[23] F. dell'Isola, P. Seppecher, M. Spagnuolo, et al., Advances in pantographic structures: design, manufacturing, models, experiments and image analyses, Contin. Mech. Thermodyn. 31 (4) (2019) 1231–1282.
[24] M. Spagnuolo, M.E. Yildizdag, U. Andreaus, A.M. Cazzani, Are higher-gradient models also capable of predicting mechanical behavior in the case of wide-knit pantographic structures? Math. Mech. Solids 1081286520937339.
[25] M.E. Yildizdag, E. Barchiesi, F. dell'Isola, Three-point bending test of pantographic blocks: numerical and experimental investigation Math. Mech. Solids 1081286520916911.
[26] P. Germain, The method of virtual power in the mechanics of continuous media, I: Second-gradient theory, Math. Mech. Complex Syst. 8 (2) (2020) 153–190.
[27] F. dell'Isola, I. Giorgio, M. Pawlikowski, N.L. Rizzi, Large deformations of planar extensible beams and pantographic lattices: heuristic homogenization, experimental and numerical examples of equilibrium, Proc. R. Soc. A Math. Phys. Eng. Sci. 472 (2185) (2016) 20150790.
[28] F. Dell'Isola, T. Lekszycki, M. Pawlikowski, R. Grygoruk, L. Greco, Designing a light fabric metamaterial being highly macroscopically tough under directional extension: first experimental evidence, Z. Angew. Math. Phys. 66 (6) (2015) 3473–3498.
[29] B. Desmorat, M. Spagnuolo, E. Turco, Stiffness optimization in nonlinear pantographic structures, Math. Mech. Solids 25 (12) (2020) 2252–2262.
[30] F.G. Vasquez, G.W. Milton, D. Onofrei, Complete characterization and synthesis of the response function of elastodynamic networks, J. Elasticity 102 (1) (2011) 31–54.
[31] I. Giorgio, A. Della Corte, F. dell'Isola, D.J. Steigmann, Buckling modes in pantographic lattices, C. R. Mec. 344 (7) (2016) 487–501.
[32] V.A. Eremeyev, F. dell'Isola, C. Boutin, D. Steigmann, Linear pantographic sheets: existence and uniqueness of weak solutions, J. Elasticity 132 (2) (2018) 175–196.
[33] U. Andreaus, M. Spagnuolo, T. Lekszycki, S.R. Eugster, A Ritz approach for the static analysis of planar pantographic structures modeled with nonlinear Euler–Bernoulli beams, Contin. Mech. Thermodyn. 30 (5) (2018) 1103–1123.
[34] R. Ghaffarivardavagh, J. Nikolajczyk, S. Anderson, X. Zhang, Ultra-open acoustic metamaterial silencer based on Fano-like interference, Phys. Rev. B 99 (2) (2019) 024302.
[35] A. Ovsianikov, A. Deiwick, S. Van Vlierberghe, P. Dubruel, L. Möller, G. Dräger, B. Chichkov, Laser fabrication of three-dimensional CAD scaffolds from photosensitive gelatin for applications in tissue engineering, Biomacromolecules 12 (4) (2011) 851–858.
[36] J. Bauer, A. Schroer, R. Schwaiger, I. Tesari, C. Lange, L. Valdevit, O. Kraft, Push-to-pull tensile testing of ultra-strong nanoscale ceramic–polymer composites made by additive manufacturing, Extreme Mech. Lett. 3 (2015) 105–112.
[37] H. Yang, G. Ganzosch, I. Giorgio, B.E. Abali, Material characterization and computations of a polymeric metamaterial with a pantographic substructure, Z. Angew. Math. Phys. 69 (4) (2018) 105.
[38] G. Flamourakis, I. Spanos, Z. Vangelatos, P. Manganas, L. Papadimitriou, C. Grigoropoulos, A. Ranella, M. Farsari, Laser-made 3D auxetic metamaterial scaffolds for tissue engineering applications, Macromol. Mater. Eng. 305 (7) (2020) 2000238.
[39] R. Wollhofen, J. Katzmann, C. Hrelescu, J. Jacak, T.A. Klar, 120 nm resolution and 55 nm structure size in STED-lithography, Opt. Express 21 (9) (2013) 10831–10840.
[40] D.C. Lam, F. Yang, A. Chong, J. Wang, P. Tong, Experiments and theory in strain gradient elasticity, J. Mech. Phys. Solids 51 (8) (2003) 1477–1508.
[41] C. Boutin, Microstructural effects in elastic composites, Int. J. Solids Struct. 33 (7) (1996) 1023–1051.
[42] E. Barchiesi, S.R. Eugster, L. Placidi, F. Dell'Isola, Pantographic beam: A complete second gradient 1D-continuum in plane, Z. Angew. Math. Phys. 70 (5) (2019) 135.
[43] A. Rafsanjani, D. Pasini, Bistable auxetic mechanical metamaterials inspired by ancient geometric motifs, Extreme Mech. Lett. 9 (2016) 291–296.
[44] D. Scerrato, I. Giorgio, Equilibrium of two-dimensional cycloidal pantographic metamaterials in three-dimensional deformations, Symmetry 11 (12) (2019) 1523.
[45] K. Roovers, N. De Temmerman, Deployable scissor grids consisting of translational units, Int. J. Solids Struct. 121 (2017) 45–61.
[46] Y. Ling, X. Zhuang, Z. Xu, Y. Xie, X. Zhu, Y. Xu, B. Sun, J. Lin, Y. Zhang, Z. Yan, Mechanically assembled, three-dimensional hierarchical structures of cellular graphene with programmed geometries and outstanding electromechanical properties, ACS Nano 12 (12) (2018) 12456–12463.
[47] M. Power, A.J. Thompson, S. Anastasova, G.-Z. Yang, A monolithic force-sensitive 3D microgripper fabricated on the tip of an optical fiber using 2-photon polymerization, Small 14 (16) (2018) 1703964.
[48] S. Palagi, D.P. Singh, P. Fischer, Light-controlled micromotors and soft microrobots, Adv. Opt. Mater. 7 (16) (2019) 1900370.